Friction **11**(2): 216–227 (2023)
https://doi.org/10.1007/s40544-021-0590-5
ISSN 2223-7690
CN 10-1237/TH
RESEARCH ARTICLE

Surroundings affect slip length dynamics in nanoscale friction through contact stiffness and damping

Simona SKURATOVSKY[1], Liron AGMON[1], Enrico GNECCO[2], Ronen BERKOVICH[1,3,*]

[1] *Department of Chemical Engineering, Ben-Gurion University of the Negev, Beer-Sheva 8410501, Israel*

[2] *Marian Smoluchowski Institute of Physics, Jagiellonian University, Lojasiewicza 11, Krakow 30-348, Poland*

[3] *Ilze Katz Institute for Nanoscience and Technology, Ben-Gurion University of the Negev, Beer-Sheva 8410501, Israel*

Received: 19 July 2021 / Revised: 04 September 2021 / Accepted: 12 December 2021

Abstract: Friction force microscopy (FFM) explores the interaction in a sliding contact on the nanoscale, providing information on the frictional dynamics and lateral contact stiffness with lattice resolution. Recent FFM measurements on a NaCl crystal immersed in liquid (ethanol) surroundings displayed an increase of the effective contact stiffness, K_{eff}, with the applied load, differently from similar measurements performed under ultra-high vacuum (UHV) conditions, where K_{eff} showed negligible load dependency. Additionally, under UHV conditions multiple slip length friction with increasing load was reported, while in ethanol surroundings only single (lattice unit length) slips were observed. Our current understanding of this behavior relates the transition from single jumps to multiple jumps dynamics to the normal load (manifested through the amplitude of the interaction potential at the contact, U_0) and to the damping of the system. Here we have incorporated the effect of the load dependency on both U_0 and K_{eff} within Prandtl–Tomlinson based simulations, accompanied by variations in the damping coefficient of the system. Introducing the experimentally observed load dependency to K_{eff} resulted indeed in single slip jumps at critical damping, while multiple slip jumps were obtained at constant K_{eff}. The average slip length increased with the normal load, particularly when the system became underdamped. Our work provides a glimpse on the relation between the characteristic observables in atomic-scale sliding friction (maximal slip forces, stiffness, and slip dynamics) with respect to their governing parameters (corrugation energy, effective stiffness, and damping). While common understanding in nanotribology relates the effect of surrounding media mainly to the interaction potential at the contact, here we show that the media can also greatly affect the elastic interaction, and consequently play an important role on the transition from single to multiple stick-slip.

Keywords: friction force microscopy (FFM); nanoscale friction; multiple jumps; Prandtl–Tomlinson model; effective stiffness; damping

1 Introduction

Friction is a phenomenon related to irreversible dissipation of energy through the dynamic interaction between two surfaces that come into contact and slide past each other. The study of friction on the nanoscale provides valuable insights on the fundamental mechanisms that govern the interaction within single junctions formed and broken between the contacting surfaces. One of the most useful approaches to probe contacts at the single asperity level is friction force microscopy (FFM), which is a straightforward extension of atomic force microscopy (AFM) [1–3]. The lateral force (friction) between a sharp tip supported by the AFM cantilever and a surface of interest is recorded, as the tip slides on the last one. The AFM is used to

*Corresponding author: Ronen BERKOVICH, E-mail: berkovir@bgu.ac.il

manipulate the base of the cantilever and to scan the surface at different rates and under various loadings. On a crystal surface these recordings provide friction maps and friction loops with lattice resolution characterized by stick-slip dynamics [4–12]. The stick-slip pattern results from the tip-surface interaction energy landscape, which consists of neighboring potential wells where stick events followed by irreversible jumps (slips) over the energy barriers separating the wells occur.

The Prandtl–Tomlinson (PT) model [13–15] is commonly used to provide a basic mechanistic framework to describe stick-slip frictional interaction [4, 6, 8, 11, 12, 16]. It accounts for the contact as a mass point particle which is elastically driven across a (load-dependent) periodic potential with the symmetry of the surface lattice. Through this portrayal, the recorded stick-slip dynamics reflects instabilities occurring during the motion of the tip between consecutive minima in the tip-surface interaction potential. Essentially, the interplay between the contributions of the potential corrugation and the elasticity accounts for the nature of the friction dynamics, i.e., continuous, or sharp transitions (may they be over a single or several lattice constants). A criterion for the transition from smooth sliding to stick-slip is set by the PT parameter, i.e., the dimensionless quantity [17]:

$$\eta = \frac{4\pi^2 U_0}{K_{\text{eff}} a^2} \tag{1}$$

This parameter physically represents the ratio between the amplitude of the interaction potential, U_0 (which is supposed to be sinusoidal), and the elastic spring energy (via K_{eff}, the effective lateral contact stiffness, and a, the lattice periodicity). If $\eta > 1$, the interaction potential dominates over the spring energy, and stick-slip motion is observed: The tip persists in the minimum of the corrugation potential until it slips to a close minimum on the lattice. If $\eta < 1$, the tip will continuously slide over the surface with no stick-slip dynamics pattern, and $\eta = 1$ marks the transition between the two regimes.

Long length jumps ("multiple" slips) over more than one lattice constant, are predicted by the PT model when η assumes high values. In the quasi-static limit of the PT model, the number of possible minima in the energy landscape can be precisely estimated according to η. As η increases, more and more potential wells become accessible to the tip, and longer and longer slips are allowed [18]. The damping coefficient γ also plays an important role in the transition from single to multiple slips. It relates to the thermal fluctuations at the contact, as indicated by the fluctuation-dissipation theorem [18–22]. Due to the coupling of the excitations of surface and tip, single slip events are preferred when the contact vibrations are overdamped and the dissipated energy rate in a slip is fast [19]. As a critical value for the damping coefficient, γ_C, one usually takes that of the harmonic oscillator corresponding to the tip decoupled from the corrugated surface potential but still subject to the elastic deformation of the contact [20, 22, 23] (see Eq. (7) below). At low damping ($\gamma < \gamma_C$), contact vibrations are underdamped, and slip can easily overshoot over two, three, and more lattice constants up to the maximum slip length allowed by η. At high damping, only single slip events will be likely observed (as the damping restrains the tip motion), even if more than two minima are present. This means that although the value of η predicts the number of minima corresponding to the given energy landscape, the quantity γ will ultimately determine the actual dynamics.

Considerable amount of FFM experiments reporting lattice resolution were performed under ultrahigh vacuum (UHV) or in other dry environments (for instance in N_2 or Ar [4, 6, 7, 9]) in order to avoid complications that may arise from the presence of capillary forces and possible contaminants. An alternative to UHV conditions consists in performing FFM experiments in liquid surroundings [10, 24–26]. First attempts to compare the stick-slip behavior observed in the two environments were performed in the case of graphene and NaCl [27, 28]. While FFM measurements on NaCl with Si tip in UHV resulted in a consistent increase of the PT parameter η with the applied load [6, 19], a non-monotonous behavior was reported for similar measurements in liquid surroundings (ethanol) [29]. In both environments the maximal stick forces, F_{max}, increased monotonously with the applied load, as was also reported for graphene in UHV and in liquid (water) [27]. K_{eff}, however, showed very little variation with the applied load in UHV for NaCl [6, 19],

though substantially growing upon measuring in liquid surroundings [28, 29]. These different behaviors in η and K_{eff} are expected to affect the friction dynamics, and indeed, under UHV, multiple jumps appeared at increasing loads on both NaCl [19] and graphite [18]. However, this was not the case for FFM data acquired on NaCl in ethanol [28, 29], where the recorded stick-slip signal corresponded to single slip lengths over a wide range of normal loads, as can be seen in Fig. 1.

In contrast with the other quantities, measuring the contact damping coefficient is very problematic since direct detection of the viscous force, $-\gamma v$ (where v is the tip velocity), requires considerably higher scanning velocities than those accessible using AFM [19, 23]. Numerical simulations aiming to explore the effect of the applied normal load, F_{N}, on the friction dynamics

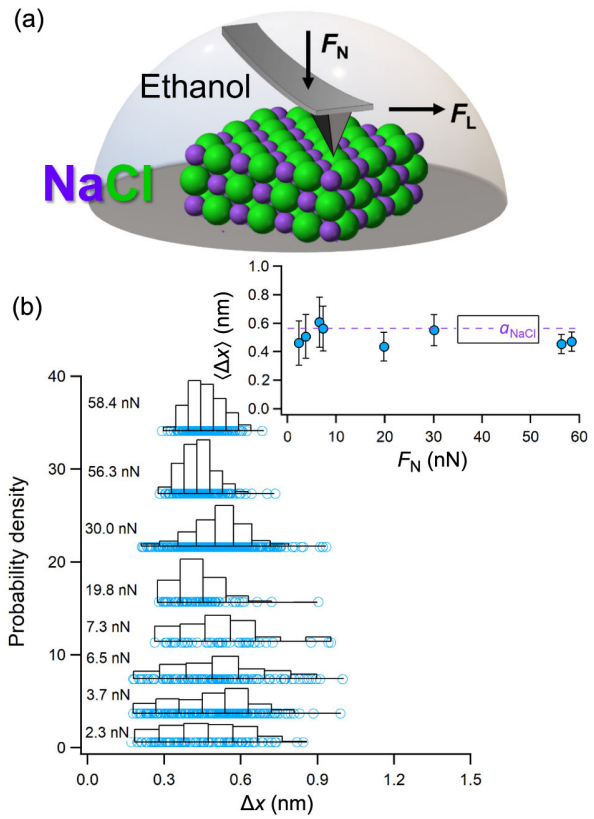

Fig. 1 Slip length obtained from NaCl measured in ethanol. (a) Schematics of the FFM measurement of NaCl immersed in ethanol. (b) Slip lengths probability distribution functions (PDFs) calculated from NaCl FFM experiments in ethanol under varying applied load (F_{N} = 2.3–58.4 nN; V = 60 nm/s). The inset shows the moments (mean and standard deviations) of the PDFs, where the periodicity of NaCl lattice (a = 0.564 nm) is plotted with a purple dashed line.

(slip lengths) through the interplay between the PT parameter and the damping coefficient can provide important insights. It must be noted that scanning velocity, temperature, and surface disorder also affect the transition from single to multiple jumps [21, 23, 30, 31], however in this study the data was obtained from experiments (and simulations) that were performed on crystal surfaces at constant velocity and temperature. By implementing the experimentally (empirically) observed dependency on the applied load in the measured lateral forces and stiffness into our simulations, we are able to reproduce the single length slip observed in the FFM measurements in ethanol. Furthermore, when holding K_{eff} constant while varying the damping, we obtain the increasing trend of multiple jumps with the applied load, which was reported for UHV-FFM measurements on NaCl.

2 Methods

FFM dynamics has been simulated with the Langevin equation within the framework of the PT model. As previously mentioned, the PT model (in 1D) depicts the elastically driven AFM tip as a mass point in a harmonic potential, $U_{\text{elastic}}(x, t)$, which is being dragged by a support moving at constant velocity V over a corrugated periodic potential, $U_{\text{interaction}}(x)$, with an amplitude U_0 and periodicity a. The total potential is thus given by

$$E(x,t) = U_{\text{interaction}}(x) + U_{\text{elastic}}(x,t) \tag{2}$$

$$E(x,t) = -U_0 \cos\left(\frac{2\pi x}{a}\right) + \frac{1}{2}K_{\text{eff}}(x - Vt)^2 \tag{3}$$

The parameter K_{eff} in Eq. (3) is the aforementioned effective stiffness of the system [32], and it is in principle load-dependent. The sinusoidal potential represents the surface-tip interaction, where x is the tip coordinate defining the one-dimensional reaction length, and t is time. The time evolution of the system can be obtained by solving Eq. (4):

$$M\ddot{x}(t) = -\gamma\dot{x}(t) - \frac{\partial E(x,t)}{\partial x} + \Gamma(t) \tag{4}$$

where M is the effective mass of the tip, γ is the aforementioned damping coefficient, and $\Gamma(t)$ is a

fluctuating random force, given by the fluctuation-dissipation theorem with $\langle \Gamma(t) \rangle = 0$, and $\langle \Gamma(t)\Gamma(t') \rangle = 2\gamma k_B T \delta(t - t')$ with k_B being Boltzmann's constant, and T the absolute temperature.

It is well-known that the amplitude of the tip-sample interaction is considerably affected by the normal force [6, 28, 33, 34], i.e., $U_0 = U_0(F_N)$, the precise relation being dependent on the geometry and elastic properties of the contacting materials. In order to comply with FFM measurements on NaCl in both UHV [6] and in ethanol [28, 29], we use the general ansatz in Eq. (5):

$$U_0(F_N) = \varepsilon \left(1 - \frac{F_N}{F_0} \right)^{\nu} \tag{5}$$

It relates the amplitude of the interaction potential to the applied load via the parameters F_0, the force at which $U_0 = 0$, ε, which defines the interaction amplitude at zero force, i.e., $\varepsilon = U_0(F_N = 0)$ and an empiric exponent ν, which is ~1 here [28, 29].

The effective spring constant, K_{eff}, was shown to increase with the applied load [16, 28, 29], meaning that $K_{eff} = K_{eff}(F_N)$. The effect of the normal load on the velocity (and temperature) dependency of nanoscale friction was recently related to the distribution of contact pressure across the interface [35]. The model by Ouyang et al. is elegant, but it requires a knowledge of parameters, such as the thermal activation rates of local bond formation/dissociation (attempting frequencies), the corresponding barrier heights for these processes, contact pressure, activation volumes, etc., that are not easily accessible experimentally. For this reason, we use also in this case an empirical power-law approximation that was already used to describe the dependency of the measured K_{eff} on the normal load [28, 29]:

$$K_{eff}(F_N) \sim K_0 + K_1 F_N^k \tag{6}$$

(where K_0, K_1, and k are fitted parameters). The damping coefficient γ is difficult to measure directly, because the damping force $-\gamma v$ is only relevant in the fast slip phase. Various estimations [5, 19, 36, 37], however, agree within an order of magnitude and yield $\gamma \sim 10^{-6}$–10^{-5} kg/s. These values are in close proximity to the critical damping of the system [20, 38, 39]:

$$\gamma_C = 2M\sqrt{\frac{K_{eff}}{M}} \tag{7}$$

Depending on the experimental conditions, the tip motion can be thus expected to be either slightly underdamped or overdamped. Furthermore, since $K_{eff} = K_{eff}(F_N)$, also $\gamma_C = \gamma_C(F_N)$.

When U_0 and K_{eff} are a priori unknown, the PT parameter η defined in Eq. (1) can be evaluated directly from measured quantities, i.e., the maximal stick forces, F_{max}, and the derivative of the (lateral) spring force F_L with respect to the support position $X = Vt$, $K_{exp} = dF_L/dX$, as in Ref. [6]:

$$\eta_{exp} = \frac{2\pi \langle F_{max} \rangle}{\langle K_{exp} \rangle a} - 1 \tag{8}$$

Once η (or η_{exp}) is known, the effective stiffness can be estimated from the local stiffness with the expression in Eq. (9) [17]:

$$K_{eff} = \left(1 + \frac{1}{\eta} \right) \langle K_{exp} \rangle \tag{9}$$

To simulate the FFM experiments, the load dependent corrugation amplitude and effective stiffness given by Eqs. (5) and (6) were substituted into the overall tip-sample interaction potential, Eq. (3), which is in turn substituted into the general equation of motion, Eq. (4). We implemented the numerical solution by separating Eq. (4) into two variable equations with first order derivatives, which we solved with Verlet integration [29, 30]. The following parameters were used for the simulations: $M = 10^{-12}$ kg [39], $T = 293$ K, $k_B T = 4.1 \times 10^{-3}$ nN·nm, $V = 60$ nm/s, and $a = 0.564$ nm. The parameters for $U_0(F_N)$ and $K_{eff}(F_N)$ were taken as the experimentally fitted values [28, 29]: $\varepsilon = 0.0143$ eV, $F_0 = -0.245$ nN, $\upsilon = 1.084$, $K_0 = 0.95$ nN/nm, $K_1 = 0.012$ nN^{1-k}/nm, and $k = 1.69$. The time step interval for the simulations was taken as 5×10^{-10} s. The resulting time dependent position trajectories, $x(t)$, were used to calculate the lateral (friction) force as $F_L = K_{eff}[Vt - x(t)]$ [19, 29].

In the simulations we explored four cases where the effective stiffness was varied with the force according to Eq. (6) or held at the constant value of $K_{eff} = 2$ nN/nm observed in UHV conditions [6], and

the damping was taken at its critical value, as defined by Eq. (7), or held constant at $\gamma = 2.83\times10^{-6}$ kg/s calculated for $K_{eff} = 2$ nN/nm (below the load dependent critical value). Figure 2 illustrates the four scenarios that we explored with the simulations: $K_{eff}(F_N)$ and $\gamma(F_N)$ (case 1, corresponding to the parameters reported for NaCl in ethanol), $K_{eff}(F_N)$ and $\gamma = 2.83\times10^{-6}$ kg/s (case 2), $K_{eff} = 2$ nN/nm and $\gamma(F_N)$ (case 3), and $K_{eff} = 2$ nN/nm and $\gamma = 2.83\times10^{-6}$ kg/s (case 4). Case 2 explores the possibility of underdamping, i.e., $\gamma = 2.83\times10^{-6}$ kg/s < $\gamma[K_{eff}(F_N)]$ for the situation in which $K_{eff} = K_{eff}(F_N)$. Under UHV, it was reported that the system goes from being underdamped into slightly overdamped with the increasing of the force [19]. This situation is reflected in case 3, while case 4 explores the possibility of the system being at critical damping.

Slip lengths from the experimental and simulated data were calculated using Hooke's law [19, 20], i.e., $\Delta x_i = (F_{i,max} - F_{i+1,min})/K_{exp,i}$, where $K_{exp,i} = (F_{i,max} - F_{i,min})/(X_i - X_{i-1})$, with $F_{i,max}$ being the i-th value of the maximal force (with the support positioned at X_i), followed by $F_{i+1,min}$, which is the minimum force after the consecutive slip (located at X_{i+1}), and $F_{i,min}$ (located at X_i) is the minimal force that precedes $F_{i,max}$. This means that each slip length is evaluated by the force drop at the slip event divided by the recorded local stiffness.

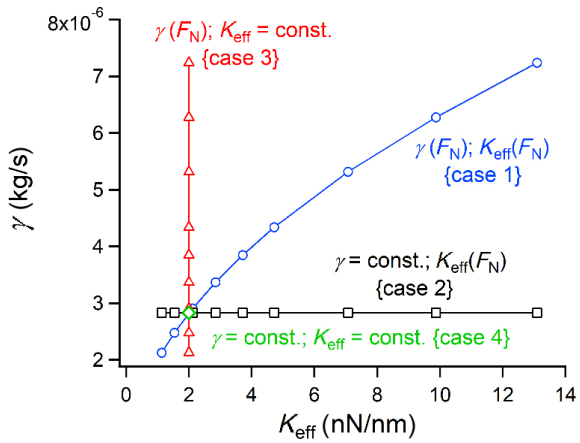

Fig. 2 Representation of the four case studies that were examined by changing K_{eff} and γ with the normal load.

3 Results and discussion

The PT parameter reported for NaCl in UHV under loads up to 91 nN reached up to $\eta = 14.5$ [19]. Comparable high values (displaying different trends) were reached for NaCl in ethanol [29]. The NaCl in UHV measurements showed increasing slip lengths, in accord with the predictions and previous observations of single slips occurring at $1 < \eta < 4.6$, double slips at $4.6 < \eta < 7.79$ and larger at $\eta > 7.79$ [18, 19], while the NaCl in ethanol showed mostly single slips events (Fig. 1(b)). This points towards the possibility that the damping in liquid surroundings is higher than in UHV. As it was previously mentioned, for NaCl K_{eff} showed very little change with the applied normal load under UHV [6, 19], while in ethanol it displayed a substantial increase [28]. These values of η and K_{eff} define the region in the parameter space, where we are interested in studying the interrelations between normal load, damping coefficient, and slip-lengths.

Figure 3(a) shows several simulated stick-slip traces under increasing normal load (from bottom to top) for case 1, where both K_{eff} and γ vary with F_N. As can be seen, the maximal slip forces and the slopes in the

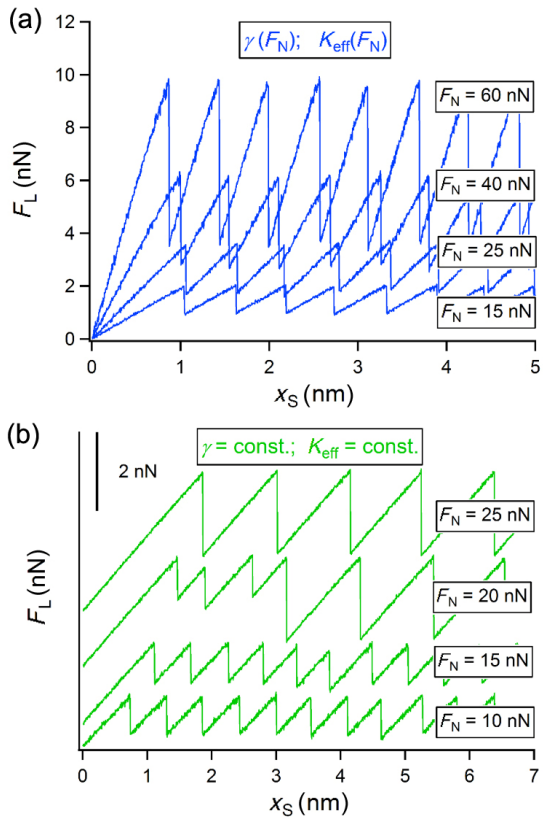

Fig. 3 FFM simulations with normal force varying and constant K_{eff} and γ. (a) Simulated force traces with $K_{eff}(F_N)$ and $\gamma(F_N)$ (case 1) at $F_N = 15$, 25, 40, and 60 nN. (b) Simulated force traces with constant K_{eff} and γ (case 4) at $F_N = 10$, 15, 20, and 25 nN.

stick-phase slopes (dF_L/dX) increase with the load, but the slip length remains constant. Some simulated stick-slip force traces in the opposite case 4, where both K_{eff} and γ are held at the previously defined fixed values are shown in Fig. 3(b). Here the increase of the maximal slip forces is also evident, however the stick-phase slopes remain constant, and traces at F_N = 20 nN display a mixed behavior of single and double slip lengths, which turn into double slips at F_N = 25 nN.

As can be seen in Fig. 4(a), the mean value of F_{max} increases with the applied load in a similar way in all four cases, with no relation to γ nor K_{eff}. This implies that mainly the corrugation term, U_0, in the free energy profile in the PT model determines $\langle F_{max} \rangle$. This behavior is in concert with previous studies that reported similarity in friction signals between FFM measurements performed in UHV and in liquid surroundings [27, 28]. In the simulations the corrugation amplitude, U_0, has been increased with F_N according to the dependency given by Eq. (5). On the other hand, the mean slope K_{exp} at the stick phase, shows a different behavior, as seen in Fig. 4(b). This behavior strongly builds upon the normal load dependency of K_{eff} assumed in the simulations. For cases 1 and 2, where $K_{eff} = K_{eff}(F_N)$, K_{exp} increases with the normal load. On the other hand, if K_{eff} is kept constant, as in cases 3 and 4, K_{exp} asymptotically tends to K_{eff}, in line with the fact that K_{exp} is equal to K_{eff} multiplied by a factor of $\eta/(\eta + 1)$. In Fig. 4(b) this is well seen above F_N = 15 nN. Note that the difference due to the load dependency of γ is negligible, which suggests that (experimentally) the damping plays almost no role not only on $\langle F_{max} \rangle$ but also on $\langle K_{exp} \rangle$.

The dependency of the normal load on U_0 and K_{eff} manifested on both F_{max} and K_{exp}, is expected to also influence the PT parameter. Figure 4(c) shows that η_{exp}, calculated using Eq. (8), is mostly affected by the effective stiffness. This could be expected from the observed trends of the maximal slip forces, which did not show any change for the four case studies (Fig. 4(a)), while K_{exp} displayed distinct different behaviors for $K_{eff}(F_N)$ and for K_{eff} = const. (Fig. 4(b)). For K_{eff} = const., η_{exp} grows with the applied load, as observed for NaCl measurements in UHV [6, 19], while for $K_{eff}(F_N)$ we observe a non-monotonous behavior of η_{exp} with the applied load similar to that reported for NaCl measurements in ethanol [29]. This is the first key conclusion of the present work.

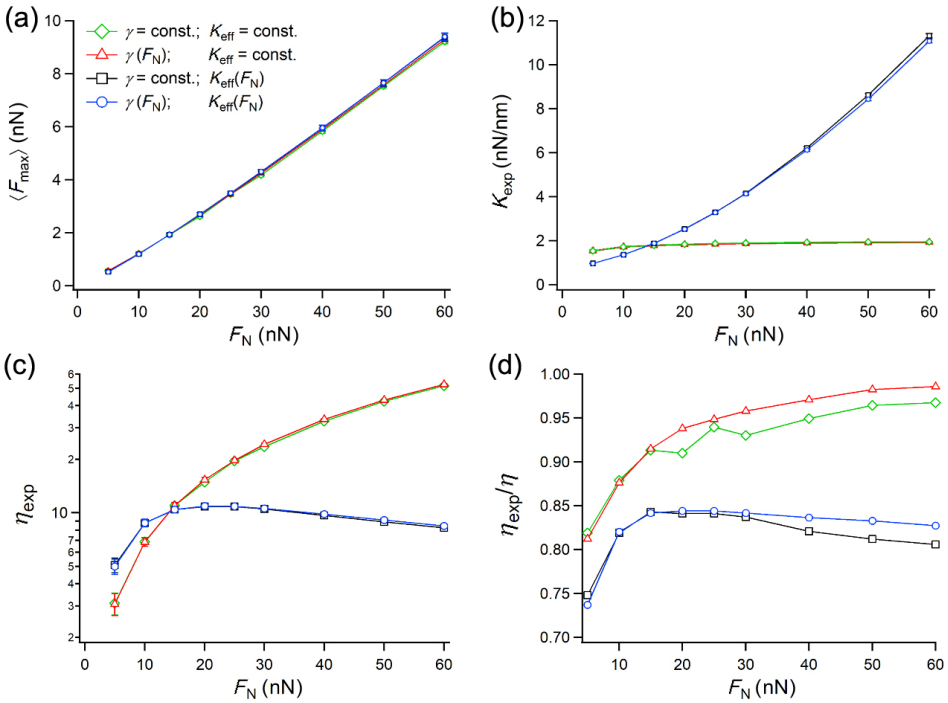

Fig. 4 Load effect for the four case-studies. (a) Mean maximal slip forces as a function of the normal load. (b) Interaction stiffness, K_{exp}, as a function of the normal load. (c) η_{exp} as a function of the normal load. (d) The ratio between η_{exp}, calculated from the experimental parameters in (a) and (b), and η calculated from U_0 and K_{eff}.

It should be noted that the expression in Eq. (8) for η_{exp} provides an approximation for η given by Eq. (1), since it is evaluated at zero temperature, while $\langle F_{max} \rangle$ is measured at finite temperature. To evaluate the deviation of η_{exp} from the actual value of η, we plotted the ratio between them as a function of the normal load in Fig. 4(d). As can be seen, when K_{eff} is constant, the differences are mild, and become less than 5% as the load increases (at $F_N > 20$ nN). When $K_{eff} = K_{eff}(F_N)$, the error is larger, yet at $F_N > 10$ nN it remains less than 20%. It is interesting to notice the effect of the damping on this ratio: at $F_N > 15$ nN, the error in η_{exp} with respect η to slightly increases. Considering these relatively moderate differences, and with the intention to approach our analysis from an experimental perspective (where the ideal U_0 and K_{eff} are not always known), we use η_{exp} instead of η in Eq. (9), and also from here onwards.

The exemplary simulated force traces shown in the opposite case studies presented in Figs. 3(a) and 3(b), indicate that the load-dependency of the damping (and phenomenologically of K_{eff}, as given by Eq. (7)) results in different slip length. We therefore calculated the slip-length distribution (normalized by the lattice constant) for each case and plotted them in Fig. 5. Case 1 shows small variation around single slip, with its distribution becoming narrower with the increase of F_N (Fig. 5(a)). Case 2 shows a transition from a single to double slip length with the increase in F_N (Fig. 5(b)). Case 3 shows transitions from single to triple slip lengths with the increase in F_N, yet the majority of slip lengths are double (Fig. 5(c)). Case 4 exhibits an increase up to seven slip lengths (Fig. 5(d)).

The means and standard deviations from the normalized slip-lengths calculated over all applied loads in the four cases are shown in Fig. 6(a). All cases display single slip events until $F_N = 15$ nN. From 20 nN and above, three cases show transitions into multi-slip length friction regime. This demonstrates the effect of the damping coefficient on the friction dynamics: When γ is related to the effective stiffness, then the system remains overdamped at increasing loads, and only single slip-events are observed (blue circles). Oppositely, when both K_{eff} and γ are constant, the long jumps made possible at increasing load (up to seven lattice constants) are observed (green diamonds). Between these two extremes: when $K_{eff}(F_N)$ and γ are constant, the jump length is smaller (black squares) compared to the situation where K_{eff} does not change, and γ increases with the load (red triangles). This is the second key result of this work.

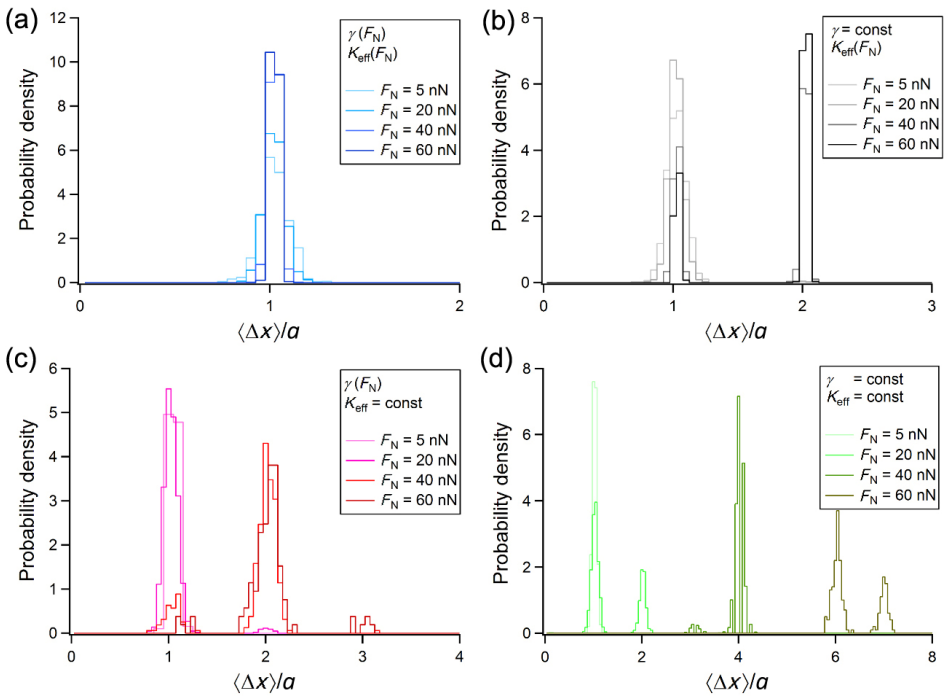

Fig. 5 Slip length (with respect to the periodicity, a) probability density functions at F_N = 5, 20, 40, and 60 nN for (a) $K_{eff}(F_N)$ and $\gamma(F_N)$, (b) $K_{eff}(F_N)$ and γ = const., (c) K_{eff} = const. and $\gamma(F_N)$, and (d) K_{eff} = const. and γ = const.

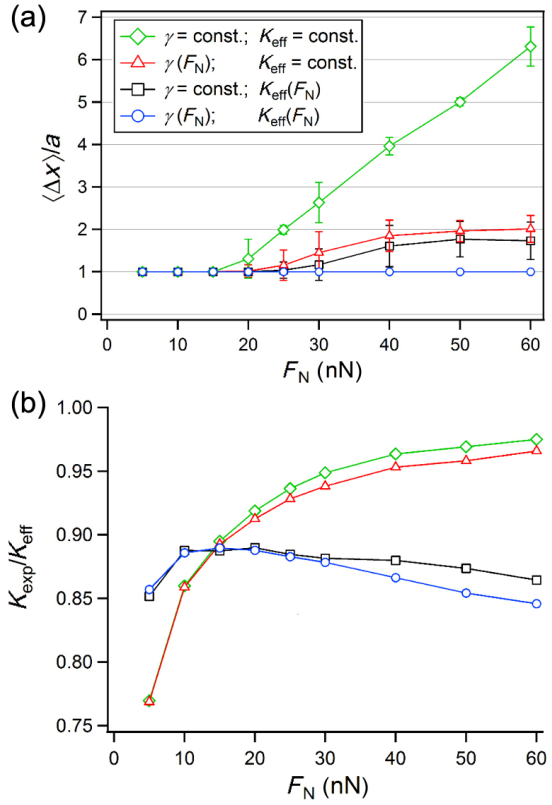

Fig. 6 Slip length and its relation to contact stiffness and damping. (a) Mean slip lengths for all examined case-studies as a function of applied normal load. (b) K_{exp}/K_{eff} (= $(1 + {}^{1}/_{\eta_{exp}})^{-1}$) as a function of the normal load.

Multiple length slips can be readily interpreted when η assumes high values at sufficiently low K_{eff} or high U_0. In the quasistatic limit, where $\partial E/\partial t = 0$, the number of solutions to $(2\pi U_0/a)\sin(2\pi x/a) = K_{eff}(Vt - x)$ defines the number of possible minima in the energy landscape. A single solution is related to smooth sliding, two solutions to a single slip length, and above three solutions to multiple slip jumps. This affects the overall contour of the energy landscape, which comprises all the corresponding possible available minima according to η [18], however, η alone does not disclose enough details on the transition between friction regimes with the applied load, which is ultimately ruled by the damping [19, 20].

We therefore plotted in Fig. 6(b) the ratio of K_{exp} to K_{eff} (= $(1 + {}^{1}/_{\eta})^{-1}$) to obtain additional information on the effect of γ through K_{eff}. It is evident that until F_N = 15 nN, where no multiple slips are observed, the difference between K_{eff} = const. and $K_{eff}(F_N)$ is hardly noticeable, while beyond this point γ becomes more relevant, and a trend similar to Fig. 6(a) (with respect to the extent of the multiple jumps occurrence) is observed. First, we see that K_{exp} asymptotically approaches K_{eff}, for the situation in which K_{eff} = const. (green diamonds and red triangles), while for $K_{eff}(F_N)$, K_{exp} remains beneath 90% of K_{eff} when it varies with F_N (black squares and blue circles). The two cases where $\gamma = \gamma(F_N)$ show a slightly smaller K_{exp}/K_{eff} ratio compared to the two cases where γ = const. (green diamonds and black squares). Although the separation at high F_N is minor, the comparable value of K_{exp}/K_{eff} ratio, or alternatively, $(1 + {}^{1}/_{\eta_{exp}})^{-1}$, can thus provide some indication on the damping state of the system (as it shows better separation compared to η_{exp} with F_N).

Figure 7 summarizes the four case-studies by plotting the η-dependency of the ratio γ/γ_C, with γ_C determined by Eq. (7) with the definition of K_{eff} characterizing each case, and η calculated with Eqs. (1), (5), and (6). This "blueprint" representation allows us to define a sort of "phase diagram" between single- and multi-slips dynamics based on the information available in Fig. 6. Below $\eta \approx 11$, all cases display single-slip dynamics although being under different damping. The situation that agrees with the observed experimental findings of NaCl in ethanol is the one where K_{eff} and γ vary with the normal load (blue squares, case 1). In this case η remains always below 11. If γ is assigned with a constant value, while K_{eff} grows with F_N (black squares, case 2) the system is first

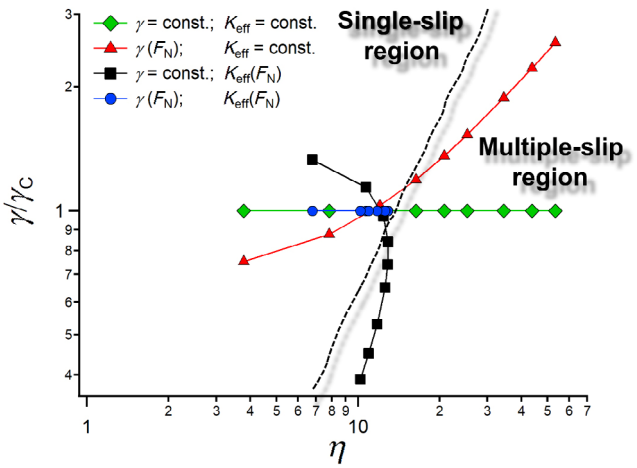

Fig. 7 Transition from single- to multi-slip in the 1D simulations resulting from the combination of the system parameters expressed via the PT parameter, η, and the damping (with respect to its phenomenological critical value), γ/γ_C.

overdamped and becomes strongly underdamped as F_N increases, with multiple (double) jumps appearing. Also in this case, the PT parameter $\eta < 11$ for all values of F_N. In the opposite case, when K_{eff} is taken as constant while γ increases with the load (red triangles, case 3), multiple (up to triple) jumps occur when $\eta > 11$ and the system is highly overdamped. Finally, when both K_{eff} and γ are kept constant (green diamonds, case 4), η grows monotonously with F_N, and multiple slips up to seven lattice constants are observed. The last two cases, for which K_{eff} = const. demonstrate the effectiveness of η in driving the system into multiple slip regardless of the damping coefficient. While the multi slip lengths that were reported for NaCl in UHV can be manifested at either relatively small underdamping, critical damping, or even at overdamping [19, 20], the negligible variation of K_{eff} [6, 19] and the increase of U_0 with the applied load, dominate the friction dynamics.

It remains to understand the physical reasons for the different behavior of K_{eff} observed on NaCl crystals with a silicon tip under UHV and at liquid surroundings (ethanol). We attribute this difference to the dissipation of heat generated in the sliding contact. Generally speaking, K_{eff} is expected to increase with the normal force F_N, since the contact area becomes larger as F_N increases [16]. However, this statement holds only if the contact temperature does not change in the stick-slip. This is possibly the case in ethanol, where convection is very efficient in removing the heat generated in the sliding contact. Indeed, K_{eff} is experimentally found to increase in this environment. In UHV, heat can only be transferred by thermal conduction far away from the contact area. This mechanism takes place essentially through the silicon tip, since NaCl is an insulator, and also slowly, since the tip is very sharp. Local heating is therefore expected, with the result of decreasing the contact stiffness at increasing values of the normal load (Young's modulus decreases with temperature and the heat released in the slip phase increases with F_N). In the case of the experiments by Socoliuc *et al.* [6] it appears that the two effects accidentally balance each other, leading to the result that K_{eff} is essentially independent of the applied load. Note that, in this context of nonequilibrium systems with small heat flows that induce spontaneous dynamic fluctuations, the concept of effective temperature may be better used [40].

4 Conclusions

We used numerical FFM simulations based on the one-dimensional PT model to study the effect of the normal load on frictional compliance (single- and multi-slip friction) through the effective lateral stiffness and damping. Current understanding of this behavior relates these friction regimes to the normal load (manifested through the corrugation energy amplitude, U_0), damping of the system, scanning velocity and temperature only. As the latter two were maintained constant, we have focused on the effect of the normal load and contact damping. In addition to the well-known influence of the normal load on the corrugation energy, we also introduced an empirical load dependency of K_{eff} on F_N based on recent experimental results of our group.

FFM measurements on NaCl in UHV [19] showed the transition from single to multiple slip with the increase of the applied load, accompanied with the increase of η. This was explained by the observed dependence of U_0 with the applied load, and the constancy of K_{eff} [6, 19], assuming that the lateral contact damping was also constant [19, 20]. In the case of NaCl in liquid surroundings (ethanol), η reaches high values, which are indeed associated with multiple slips, however, by introducing a load dependence into the damping, via K_{eff}, we observe from our 1D simulations that the lateral vibrations remain damped with the increase of loading force (and η), resulting with the single slips (that were also observed experimentally). Considering that the thermal conductivity of ethanol (~0.15 W/(m·K) [41]) is much lower than those of silicon (~150 W/(m·K) [42]) and NaCl (~6 W/(m·K) [43]), and convection is much more efficient than thermal conduction in liquids, it is not excluded that a considerable fraction of heat is released into the liquid environment. This possibility is fully confirmed by the different frictional response observed in ethanol and in UHV. In the liquid environment the contact stiffens with the applied load, and the system remains damped. Opposingly, under UHV conditions, the heat

is dissipated into the contact, and makes it less stiff. As a result, the local stiffness appears to change very little with the applied load [6], and the damping of the system varies from being somewhat underdamped into overdamped [19, 20]. Two out of the four case-studies explored here were quite close to experimental results of FFM measurements on NaCl crystal in UHV and in liquid surroundings. The use of 1D PT model enabled to gain insight on the roles of local stiffness and interaction energies, however, in practice the situation may be more complicated [44]. It should be also noted that two important aspects regarding the damping should be considered. First, damping is particularly influential in the 1D model, which was implemented here in the study of the slip length since it regulates the energy flux through the single reaction coordinate [23]. Second, here we used the commonly accepted form for the damping definition as a free oscillator [8, 12, 19, 20, 22, 38, 39]. However, a more accurate description of the damping should consider the contribution of the curvature of the potential well in which the slip ends as noticed by Fajardo and Mazo in previous work on this topic [31]. Summing up the two contributions, K_{eff} in Eq. (7) will be approximately replaced with $K_{\text{eff}}(1 + \eta)$ for a slip and with more complex expressions for multiple slip, where different "landing points" are present. In 2D the situation is made even more complicated by the zigzag motion of the tip, and a meaningful definition of γ_{C} must also take into account the direction along which the landing point is reached. Yet, the physical parameter governing the dissipation process is γ, and here we have shown that experimental results in different environments can only be reproduced assuming that γ can change with the applied load. Taking the critical value of this parameter for a free oscillator as reference is the simplest approach allowing to shed light on a problem, which would also require more experimental data for being parameterized more accurately.

Acknowledgements

R.B. and E.G are grateful for the generous financial support of Deutsche Forschungsgemeinschaft (No. DFG GN 92/16-1).

References

[1] Mate C M, McClelland G M, Erlandsson R, Chiang S. Atomic-scale friction of a tungsten tip on a graphite surface. *Phys Rev Lett* **59**: 1942–1945 (1987)

[2] Bhushan B, Israelachvili J N, Landman U. Nanotribology: Friction, wear and lubrication at the atomic-scale. *Nature* **374**: 607–616 (1995)

[3] Carpick R W, Salmeron M. Scratching the surface: Fundamental investigations of tribology with atomic force microscopy. *Chem Rev* **97**(4): 1163–1194 (1997)

[4] Gnecco E, Bennewitz R, Gyalog T, Loppacher C, Bammerlin M, Meyer E, Güntherodt H J. Velocity dependence of atomic friction. *Phys Rev Lett* **84**(6): 1172–1175 (2000)

[5] Sang Y, Dubé M, Grant M. Thermal effects on atomic friction. *Phys Rev Lett* **87**(17): 174301 (2001)

[6] Socoliuc A, Bennewitz R, Gnecco E, Meyer E. Transition from stick-slip to continuous sliding in atomic friction: Entering a new regime of ultralow friction. *Phys Rev Lett* **92**(13): 134301 (2004)

[7] Dienwiebel M, Verhoeven G S, Pradeep N, Frenken J W M, Heimberg J A, Zandbergen H W. Superlubricity of graphite. *Phys Rev Lett* **92**(12): 126101 (2004)

[8] Hölscher H, Ebeling D, Schwarz U D. Friction at atomic-scale surface steps: Experiment and theory. *Phys Rev Lett* **101**(24): 246105 (2008)

[9] Filleter T, Bennewitz R. Structural and frictional properties of graphene films on SiC(0001) studied by atomic force microscopy. *Phys Rev B* **81**: 155412 (2010)

[10] Labuda A, Paul W, Pietrobon B, Lennox R B, Grütter P H, Bennewitz R. High-resolution friction force microscopy under electrochemical control. *Rev Sci Instrum* **81**(8): 083701 (2010)

[11] Jansen L, Hölscher H, Fuchs H, Schirmeisen A. Temperature dependence of atomic-scale stick-slip friction. *Phys Rev Lett* **104**(25): 256101 (2010)

[12] Pawlak R, Ouyang W G, Filippov A E, Kalikhman-Razvozov L, Kawai S, Glatzel T, Gnecco E, Baratoff A, Zheng Q S, Hod O, *et al*. Single-molecule tribology: Force microscopy manipulation of a porphyrin derivative on a copper surface. *ACS Nano* **10**(1): 713–722 (2016)

[13] Prandtl L. Ein gedankenmodell zur kinetischen theorie der festen körper. *Z Angew Math Mech* **8**(2): 85–106 (1928)

[14] Tomlinson G A. CVI. A molecular theory of friction. *Lond Edinb Dublin Philos Mag J Sci* **7**(46): 905–939 (1929)

[15] Popov V L, Gray J A T. Prandtl-tomlinson model: History and applications in friction, plasticity, and nanotechnologies. *ZAMM J Appl Math Mech / Zeitschrift Für Angewandte Math Und Mech* **92**(9): 683–708 (2012)

[16] Mazo J J, Dietzel D, Schirmeisen A, Vilhena J G, Gnecco E. Time strengthening of crystal nanocontacts. *Phys Rev Lett* **118**(24): 246101 (2017)

[17] Gnecco E, Bennewitz R, Gyalog T, Meyer E. Friction experiments on the nanometer scale. *J Phys Condens Matter* **13**(31): R619 (2001)

[18] Medyanik S N, Liu W K, Sung I H, Carpick R W. Predictions and observations of multiple slip modes in atomic-scale friction. *Phys Rev Lett* **97**(13): 136106 (2006)

[19] Roth R, Glatzel T, Steiner P, Gnecco E, Baratoff A, Meyer E. Multiple slips in atomic-scale friction: An indicator for the lateral contact damping. *Tribol Lett* **39**(1): 63–69 (2010)

[20] Gnecco E, Roth R, Baratoff A. Analytical expressions for the kinetic friction in the Prandtl-Tomlinson model. *Phys Rev B* **86**(3): 035443 (2012)

[21] Nakamura J, Wakunami S, Natori A. Double-slip mechanism in atomic-scale friction: Tomlinson model at finite temperatures. *Phys Rev B* **72**(23): 235415 (2005)

[22] van Baarle D W, Krylov S Y, Beck M E S, Frenken J W M. On the non-trivial origin of atomic-scale patterns in friction force microscopy. *Tribol Lett* **67**: 15 (2019)

[23] Dong Y L, Perez D, Voter A F, Martini A. The roles of statics and dynamics in determining transitions between atomic friction regimes. *Tribol Lett* **42**(1): 99–107 (2011)

[24] Ohnesorge F, Binnig G. True atomic resolution by atomic force microscopy through repulsive and attractive forces. *Science* **260**(5113): 1451–1456 (1993)

[25] Pina C M, Miranda R, Gnecco E. Anisotropic surface coupling while sliding on dolomite and calcite crystals. *Phys Rev B* **85**(7): 073402 (2012)

[26] Robinson B J, Kay N D, Kolosov O V. Nanoscale interfacial interactions of graphene with polar and nonpolar liquids. *Langmuir* **29**(25): 7735–7742 (2013)

[27] Vilhena J G, Pimentel C, Pedraz P, Luo F, Serena P A, Pina C M, Gnecco E, Pérez R. Atomic-scale sliding friction on graphene in water. *ACS Nano* **10**(4): 4288–4293 (2016)

[28] Agmon L, Shahar I, Yosufov D, Pimentel C, Pina C M, Gnecco E, Berkovich R. Estimation of interaction energy and contact stiffness in atomic-scale sliding on a model sodium chloride surface in ethanol. *Sci Rep* **8**: 4681 (2018)

[29] Skuratovsky S, Agmon L, Berkovich R. Comparative study of dimensionality and symmetry breaking on nanoscale friction in the Prandtl–tomlinson model with varying effective stiffness. *Tribol Lett* **68**(4): 113 (2020)

[30] Tshiprut Z, Zelner S, Urbakh M. Temperature-induced enhancement of nanoscale friction. *Phys Rev Lett* **102**(13): 136102 (2009)

[31] Fajardo O Y, Mazo J J. Effects of surface disorder and temperature on atomic friction. *Phys Rev B* **82**(3): 035435 (2010)

[32] Carpick R W, Ogletree D F, Salmeron M. Lateral stiffness: A new nanomechanical measurement for the determination of shear strengths with friction force microscopy. *Appl Phys Lett* **70**(12): 1548–1550 (1997)

[33] Zhong W, Tománek D. First-principles theory of atomic-scale friction. *Phys Rev Lett* **64**(25): 3054–3057 (1990).

[34] Zaloj V, Urbakh M, Klafter J. Modifying friction by manipulating normal response to lateral motion. *Phys Rev Lett* **82**(24): 4823–4826 (1999)

[35] Ouyang W G, Cheng Y, Ma M, Urbakh M. Load-velocity-temperature relationship in frictional response of microscopic contacts. *J Mech Phys Solids* **137**: 103880 (2020)

[36] Reinstädtler M, Rabe U, Scherer V, Hartmann U, Goldade A, Bhushan B, Arnold W. On the nanoscale measurement of friction using atomic-force microscope cantilever torsional resonances. *Appl Phys Lett* **82**(16): 2604–2606 (2003)

[37] Reimann P, Evstigneev M. Nonmonotonic velocity dependence of atomic friction. *Phys Rev Lett* **93**(23): 230802 (2004)

[38] Hölscher H, Schwarz U D, Wiesendanger R. Modelling of the scan process in lateral force microscopy. *Surf Sci* **375**(2–3): 395–402 (1997)

[39] Steiner P, Roth R, Gnecco E, Baratoff A, Maier S, Glatzel T, Meyer E. Two-dimensional simulation of superlubricity on NaCl and highly oriented pyrolytic graphite. *Phys Rev B* **79**(4): 045414 (2009)

[40] Cugliandolo L F, Kurchan J, Peliti L. Energy flow, partial equilibration, and effective temperatures in systems with slow dynamics. *Phys Rev E* **55**(4): 3898–3914 (1997)

[41] Vargaftik N B. *Handbook of Physical Properties of Liquids and Gases*. Berlin, Heidelberg: Springer Berlin Heidelberg, 1975.

[42] Glassbrenner C J, Slack G A. Thermal conductivity of silicon and germanium from 3°K to the melting point. *Phys Rev* **134**(4A): A1058–A1069 (1964)

[43] Håkansson B, Andersson P. Thermal conductivity and heat capacity of solid NaCl and NaI under pressure. *J Phys Chem Solids* **47**(4): 355–362 (1986)

[44] Maier S, Sang Y, Filleter T, Grant M, Bennewitz R, Gnecco E, Meyer E. Fluctuations and jump dynamics in atomic friction experiments. *Phys Rev B* **72**(24): 245418 (2005)

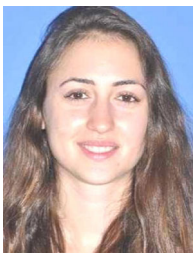

Simona SKURATOVSKY. She received her bachelor and master degrees in chemical engineering from Ben-Gurion University of the Negev, Israel, in 2017 and 2021, respectively. Her research interests include numerical aspects of load effect in nanotribology.

Ronen BERKOVICH. He received his bachelor degree in chemical engineering from the Technion – Israel Institute of Technology, Israel, in 2002, and his Ph.D. degree in chemical physics from Tel-Aviv University, Israel, in 2011. He joined the Department of Chemical Engineering at Ben-Gurion University of the Negev, Israel, as a faculty member from 2013. His researches focus on nanoscale physical mechanics, nanotribology, and single molecule biophysics.

Enrico GNECCO. He received his Ph.D. degree in physics at University of Genova, Italy, in 2001. He joined the Department of Physics at Jagiellonian University Krakow, Poland, as a faculty member. His research focuses on atomic-scale sliding friction in different environmental conditions, scanning probe microscopy manipulation, contact mechanics, and abrasive wear processes on the nanoscale.